

3D-FREE MEETS 3D PRIORS: NOVEL VIEW SYNTHESIS FROM A SINGLE IMAGE WITH PRETRAINED DIFFUSION GUIDANCE

Taewon Kang, Divya Kothandaraman, Dinesh Manocha, Ming C. Lin*

University of Maryland at College Park, United States

{taewon, dkr, dmanocha, lin}@umd.edu

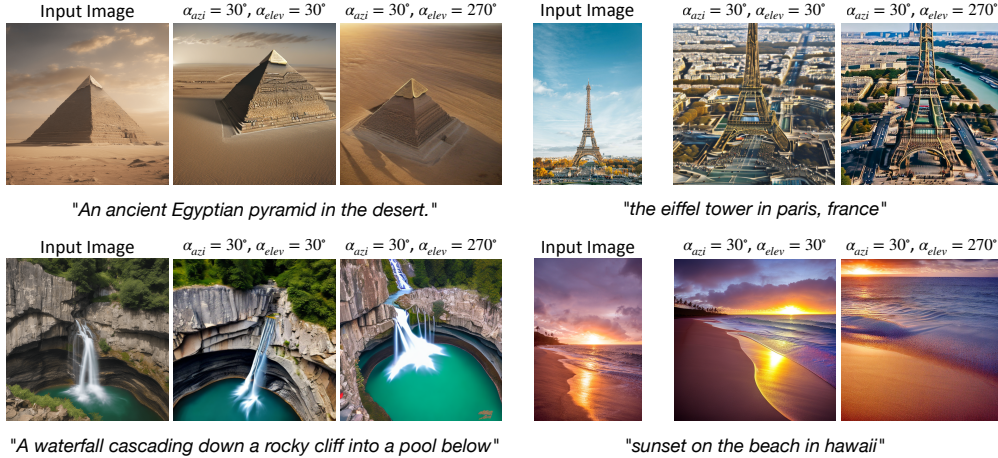


Figure 1: Our model can generate camera-controlled images at specified azimuth and elevation angles for diverse and complex scenes, without the need for additional 3D datasets or extensive training.

ABSTRACT

Recent 3D novel view synthesis (NVS) methods are limited to single-object-centric scenes and struggle with complex environments. They often require extensive 3D data for training, lacking generalization beyond the training distribution. Conversely, 3D-free methods can generate text-controlled views of complex, in-the-wild scenes using a pretrained stable diffusion model without the need for a large amount of 3D-based training data, but lack camera control. In this paper, we introduce a method capable of generating camera-controlled viewpoints from a single input image, by combining the benefits of 3D-free and 3D-based approaches. Our method excels in handling complex and diverse scenes without extensive training or additional 3D and multiview data. It leverages widely available pretrained NVS models for weak guidance, integrating this knowledge into a 3D-free view synthesis approach to achieve the desired results. Experimental results demonstrate that our method outperforms existing models in both qualitative and quantitative evaluations, providing high-fidelity and consistent novel view synthesis at desired camera angles across a wide variety of scenes.

1 INTRODUCTION

Novel-view synthesis plays a pivotal role in numerous real-world applications, including 3D environments, augmented reality (AR), virtual reality (VR), and autonomous driving. Recent advancements in diffusion-based methods, such as Zero-1-to-3 (Zero123) Liu et al. (2023a) and

*Corresponding author

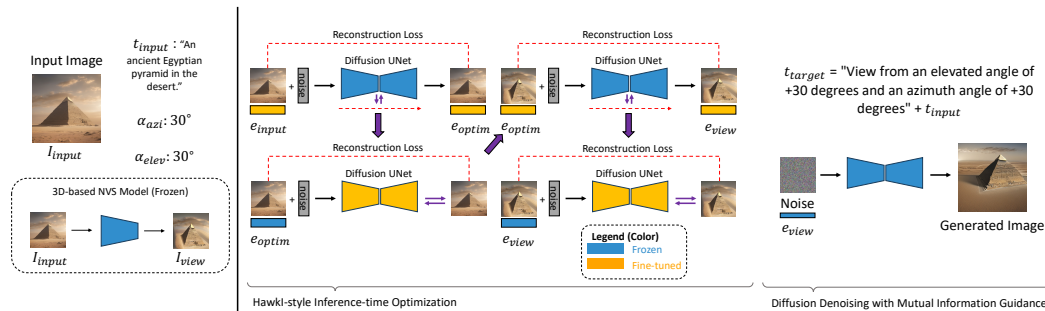


Figure 2: **Method.** Our method generates a high fidelity camera controlled novel viewpoint of a single image I_{input} , its text description and designated angle information. It infuses prior information from pre-trained NVS models into the text to image stable diffusion architecture in a 3D-free inference-time optimization procedure.

Zero123++ Shi et al. (2023a), along with NeRFs Tancik et al. (2022); Zhou & Tulsiani (2023) and Gaussian Splatting Li et al. (2024); Zhu et al. (2023), have significantly propelled the field forward. These techniques enable the specification of camera angles and the sampling of novel-view images from precise viewpoints. However, diffusion-based methods remain largely object-centric and may struggle to generalize to complex scenes with intricate backgrounds. They also require extensive 3D object datasets for training. In contrast, NeRF and Gaussian Splatting methods can handle complex scenes but depend on multi-view information to construct 3D models. Therefore, achieving novel-view synthesis from a single image in a data-efficient manner, without relying on additional 3D, multi-view, or depth information, is highly advantageous.

Conversely, 3D-free methods like HawkI Kothandaraman et al. (2023) intelligently extract the rich 3D knowledge embedded in text-to-2D image diffusion models, such as stable diffusion Rombach et al. (2022); Podell et al. (2023), to generate text-controlled views from complex, real-world input images without needing additional multi-view or 3D information for fine-tuning or inference. However, these methods lack the ability to precisely control camera angles when generating novel-view images. Ideally, we aim for both data-efficient novel view synthesis and camera controllability, which is the primary focus of this paper.

We begin by analyzing how well CLIP understands the 3D space and the benefits of guidance images for 3D-free methods like HawkI. Using these insights, along with the established knowledge that 3D-based methods such as HawkI enable precise camera control and 3D-free methods like Zero123++ offer generalizability and data efficiency, we propose a simple approach for novel-view synthesis that generates camera-controlled novel views at specified azimuth and elevation angles from a single input image, without requiring 3D datasets or extensive training.

Our method utilizes information from off-the-shelf pretrained 3D-based models like Zero123++ Shi et al. (2023a) in conjunction with the pretrained stable diffusion model. It follows a 3D-free HawkI-style inference-time optimization procedure to achieve the desired results. We validate our approach through extensive qualitative and quantitative comparisons across various metrics that assess text consistency and fidelity.

To summarize our contributions, we (1) we analyze how well the CLIP model understands the 3D space and the usefulness of guidance image in 3D-free methods, (2) present a simple approach that uses 3D-priors within 3D-free 2D-based approaches for novel view synthesis, with precise camera control, that works well for complex image with multiple objects, backgrounds, etc.

2 PRIOR WORK ON 3D AND 3D-FREE APPROACHES FOR NVS

Recent research has increasingly focused on novel view synthesis using diffusion models Chen et al. (2021); Mildenhall et al. (2021); Shi et al. (2021). Approaches for 3D generation Chen et al. (2024); Lin et al. (2023); Poole et al. (2022); Raj et al. (2023); Xu et al. (2023); Gao et al. (2024) often rely on text for reconstruction and require substantial multi-view and 3D data Shi et al. (2023b); Wang & Shi (2023); Yang et al. (2024); Liu et al. (2023b); Höllein et al. (2024) for supervised learning.

For instance, Zero123 Liu et al. (2023a), Magic123 Qian et al. (2023), and Zero123++ Shi et al. (2023a) utilize a pre-trained stable diffusion model Rombach et al. (2022) combined with 3D data to learn various camera viewpoints. However, they are extremely data hungry, meaning that they need extensive multi-view and 3D data to train on. Additionally, most state-of-the-art view synthesis algorithms are largely object-centric, and may not work well on complex scenes containing multiple objects or background information. This is due to the domain gap between the 3D objects data that they are typically trained on, and the inferencing image.

Free3D Zheng & Vedaldi (2024) introduces an efficient method for synthesizing accurate 360-degree views from a single image without 3D representations. By incorporating the Ray Conditioning Normalization (RCN) layer into 2D image generators, it encodes the target view’s pose and enhances view consistency with lightweight multi-view attention layers and noise sharing. However, it still requires training on large-scale 3D datasets like Objaverse and multi-view information, and it cannot include background transformations. DreamFusion Poole et al. (2022) presents a Text-to-3D method using a NeRF and a Diffusion Model-based Text-to-2D model. It introduces a probability density distillation loss, allowing the 2D Diffusion Model to optimize image generation without needing 3D data or model modifications. DreamFusion’s key contributions are creating Text-to-3D models without 3D dataset training and utilizing a Diffusion Model. However, it cannot transform images with backgrounds or introduce elevation changes in camera-controlled images. HawkI Kothandaraman et al. (2023) synthesizes high-quality aerial view images using text and a single input image without 3D or multi-view information. It employs a pretrained text-to-2D Stable Diffusion model, achieving a balance between aerial view consistency and input image fidelity through test-time optimization and mutual information-based inference. However, HawkI struggles with controlling camera angles, detailed feature generation, and maintaining view consistency.

3 UNDERSTANDING 2D MODELS AND THE 3D SPACE

3.1 HOW WELL DO CLIP MODELS UNDERSTAND THE 3D-SPACE?

This section examines how well CLIP models understand 3D space by focusing on the 3D-free method, HawkI Kothandaraman et al. (2023). HawkI uses classical computer vision techniques to generate aerial view images from ground view images via a homography transformation, which serves as the guidance image for the diffusion model. Our hypothesis is that HawkI’s ability to perform viewpoint transformations without 3D data relies on this homography image.

We conducted an experiment where the homography image was omitted to see if CLIP could generate camera-controlled images without it. Detailed angle instructions were still provided in the target text description. Our results showed that CLIP could not independently generate consistent viewpoints, highlighting the importance of 3D guidance images.

In the experiment, different pyramids, waterfalls, and houses were generated inconsistently, and camera control angles were not accurately followed. This demonstrates that CLIP struggles with 3D comprehension and validates the necessity of 3D guidance images. Figure 3 illustrates these findings.

3.2 IMPORTANCE OF GUIDANCE IMAGE IN 3D-FREE METHODS

Our previous analysis revealed that the CLIP model without a guidance image struggles to understand 3D space, resulting in inconsistent images. Conversely, HawkI with a guidance image cannot perform transformations from various camera viewpoints. This raises the question of what kind of guidance image is suitable for 3D-free camera control.

We conduct experiments using the images generated using the pretrained Zero123++ Shi et al. (2023a) model for guidance. In our experiments, the target text specified the desired transformation angles, but the guidance images had different angles. i.e. the guidance images introduced incorrect viewpoints. When generating an image at a $(30^\circ, 30^\circ)$ angle, the model followed the guidance image’s suggestion, regardless of the text input. This indicates that the model benefits from the information in the 3D-derived guidance image, and that the guidance image is not simply a source of extra variance. Our experiment confirms the importance of guidance images in camera control, validating our methodology. Figure 4 illustrates these findings.

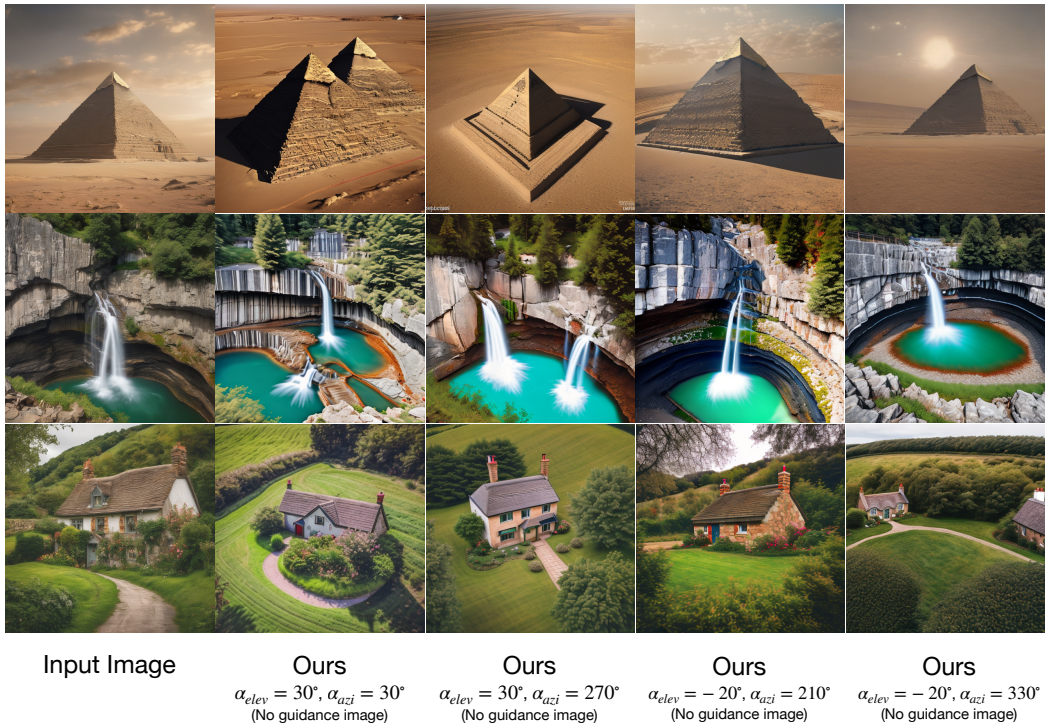


Figure 3: **Analysis of how well CLIP understands the 3D space** In this experiment, we generate camera control images for specific angles without using any guidance image.

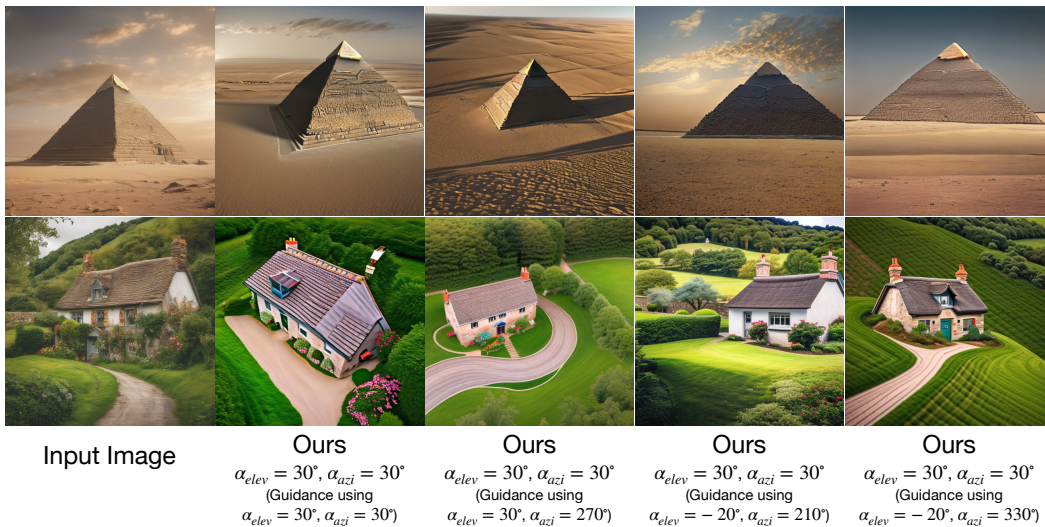


Figure 4: **Using an image with an incorrect viewpoint as the guidance image** In this experiment, we examine how the results are derived when an incorrect viewpoint image is used as a guidance image.

4 3D-FREE + 3D PRIORS FOR NOVEL-VIEW SYNTHESIS

We present a simple method (Figure 2) for data-efficient text and camera-controlled novel-view synthesis from a single input image (I_{input}) and its text description (t_{input}) (e.g., “An ancient Egyptian pyramid in the desert,” obtained using the BLIP-2 Li et al. (2023) model). Our model eliminates the need for training data, 3D data, or multi-view data. Instead, it utilizes a pretrained text-to-2D image

stable diffusion model as a strong prior, along with pretrained novel-view synthesis (NVS) models, e.g. Zero123++ for guidance. Our method combines information from the pretrained NVS model and performs a rapid inference-time optimization and inference routine, following a HawkI-style inference approach, to generate novel-view images of any given in-the-wild complex input scene at specified elevation (α_{elev}) and azimuth angles (α_{azi}).

Inference-time Optimization We employ a pretrained NVS model G to obtain a weak prediction, I_{view} , of I_{input} at $(\alpha_{elev}, \alpha_{azi})$. This prediction is represented as $I_{view} = G(I_{input}, \alpha_{elev}, \alpha_{azi})$. Although I_{view} is not a fully accurate depiction of the desired target, it provides weak or pseudo guidance for the model regarding the content and direction of the desired viewpoint transformation. Subsequently, we utilize the pretrained text-to-image stable diffusion model to perform inference-time optimization.

Specifically, initially, we enhance the CLIP embedding for t_{input} with I_{input} to derive e_{optim} (optimized CLIP text-image embedding from e_{input} , which is the CLIP test embedding for t_{input}), which is optimized to most accurately reconstruct I_{input} :

$$\min_{e_{optim}} \sum_{t=T}^0 L(f(x_t, t, e_{optim}; \theta), I_{input}) \quad (1)$$

Subsequently, the LoRA layers (with parameters θ_{LoRA}) within the cross-attention layers of the diffusion model are fine-tuned at e_{optim} to replicate I_{input} , employing the diffusion denoising loss function,

$$\min_{\theta_{LoRA}} \sum_{t=T}^0 L(f(x_t, t, e_{optim}; \theta), I_{input}) \quad (2)$$

while keeping the rest of the UNet model unchanged. This process is then iterated for I_{view} , where e_{optim} is again refined to e_{view} to best reconstruct I_{view} . Following this, the LoRA layers are adjusted to capture the nuances of the weak guidance image I_{view} , guiding the transformation towards the desired outcome.

Thus, the predicted image from the 3D-based NVS method, Zero123++, serves as weak or pseudo guidance. The optimization strategy conditions the embedding space with knowledge related to the input image and its view variants. The guidance image prior increases the variance of the diffusion model, facilitating view transformation and providing a direction for viewpoint transformation.

Inference To generate the camera-controlled image with designated elevation (α_{elev}) and azimuth angles (α_{azi}), we use the target text description t_{target} , which varies according to the corresponding α_{elev} and α_{azi} . For instance, if $\alpha_{elev} = 30^\circ$ and $\alpha_{azi} = 30^\circ$, t_{target} can be formatted as "View from an elevated angle of +30 degrees and an azimuth angle of +30 degrees" + t_{input} (e.g., "View from an elevated angle of +30 degrees and an azimuth angle of +30 degrees, An ancient Egyptian pyramid in the desert."). Next, we use the finetuned diffusion model to generate the target image using t_{target} , along with mutual information guidance Kothandaraman et al. (2023), which enforces similarity between the contents of the generated and input images.

5 EXPERIMENTS AND RESULTS

Datasets We utilize the HawkI-Syn Kothandaraman et al. (2023) and HawkI-Real Kothandaraman et al. (2023) datasets that feature complex scenes with multiple foreground objects and background. Both datasets provide images and text prompts to the model. Explain the subset you used for your results, how you created the, how many images per sample you used for evaluation, etc.

Baselines We compare our method with state-of-the-art view synthesis methods: Zero123++ Shi et al. (2023a) and Stable Zero123 for 3D-based methods and HawkI Kothandaraman et al. (2023) for 3D-free method.

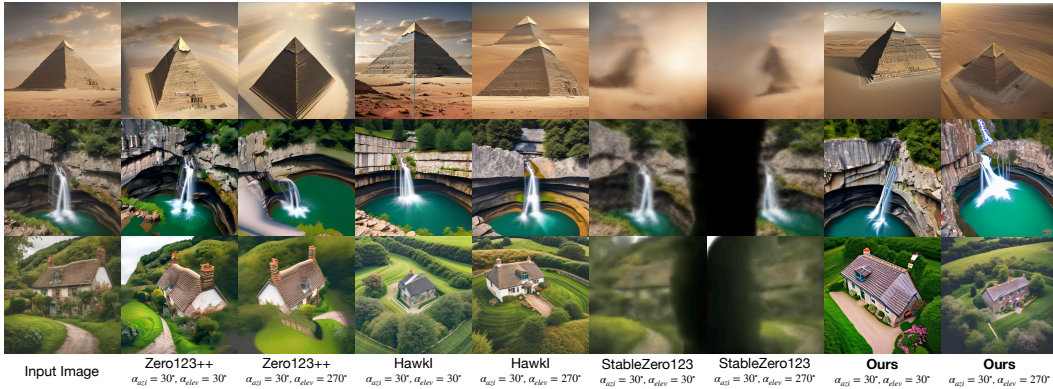


Figure 5: **Results on HawkI-Syn.** Comparisons between the state-of-the-art view synthesis models, Zero123++, HawkI, Stable Zero123, and our method highlights the superior performance of our model in terms of background inclusion, view consistency, and the accurate representation of target elevation and azimuth angles.

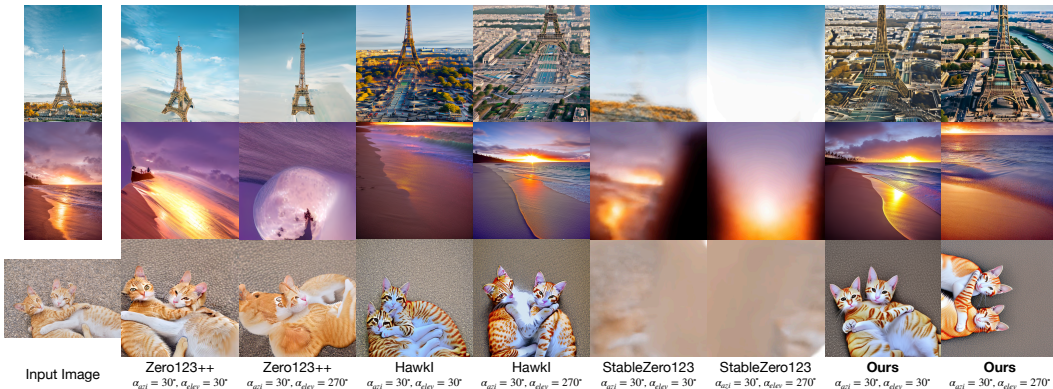


Figure 6: **Results on HawkI-Real.** Comparisons between the state-of-the-art view synthesis models, Zero123++, HawkI, Stable Zero123, and our method highlights the superior performance of our model in terms of background inclusion, view consistency, and the accurate representation of target elevation and azimuth angles.

Implementation Details We employ the stable diffusion 2.1 model as the backbone for all our experiments and results. To generate the pseudo guidance images for different viewpoints, we use the pretrained Zero123++ Shi et al. (2023a) model. All images except those in HawkI-Real dataset are used at a resolution of 512×512 . For I_{input} , we train the text embedding for 1,000 iterations with the learning rate of $1e - 3$ and the diffusion model for 500 iterations with the learning rate of $2e - 4$. Training the text embedding for 1,000 iterations guarantees that the text embedding e_{optim} is not too close to the e_{input} , avoiding bias towards I_{input} . Likewise, it is not too distant from e_{input} , allowing the text embedding space to capture the characteristics of I_{input} . Regarding I_{view} , we trained the text embedding for 500 iterations and the diffusion UNet for 250 iterations. We aim for e_{view} to be near e_{optim} and limit the diffusion model training to 250 iterations to prevent overfitting to I_{view} . The purpose of I_{view} is to introduce variability and provide pseudo supervision rather than accurately approximating the camera control. We set the mutual information guidance hyperparameter to $1e - 6$ and conduct inference over 50 steps.

5.1 QUALITATIVE ANALYSIS

We evaluate our method on four distinct viewpoints:

$$\{(\alpha_{elev}, \alpha_{azi}) \mid (30^\circ, 30^\circ), (-20^\circ, 210^\circ), (30^\circ, 270^\circ), (-20^\circ, 330^\circ)\}.$$

Our model is able to generate distinct viewpoints in the camera control to ensure consistency across generated views. Details are mentioned in the Zero123++ Shi et al. (2023a). We present qualitative



Figure 7: **More results on HawkI-Syn.** We present additional comparison results on HawkI-Syn for the angles of $(-20^\circ, 210^\circ)$ and $(-20^\circ, 330^\circ)$. Our model consistently produces view synthesis images that maintained background inclusion and view consistency, accurately mirroring the target elevation and azimuth angles. Notably, StableZero123 exhibits instability in its results. It’s important to highlight that this task specifically addresses *negative azimuth angles*. HawkI, for instance, fails to capture the correct camera elevation and is limited to generating aerial views. Zero123++ is capable of handling both elevation and azimuth but falls short in integrating background elements and intricate details, as also observed in previous outcomes. For example, when presented with an image of a pyramid casting a shadow, Zero123++ darkens the pyramid but fails to render the shadow accurately. This shortcoming is also apparent in images of a waterfall and a house. In the waterfall task within the specified azimuth range, Zero123++ produces an indistinct shape rather than a clear environment where water and lake are visible from below the rocks. Similarly, for the house image, it generates an incomplete image with gray patches. Conversely, our model not only captures the shadow details of the pyramid but also accurately renders the environment in the waterfall image, ensuring visibility of water and lake from beneath the rocks. Additionally, it adeptly incorporates details and backgrounds from multiple perspectives.

representative results and comparisons with Zero123++ Shi et al. (2023a), HawkI Kothandaraman et al. (2023), and StableZero123 at camera angles of $(30^\circ, 30^\circ)$ and $(30^\circ, 270^\circ)$ in Figures 5 and 6. Our method demonstrates superior scene reconstruction from all viewpoints compared to previous works. Specifically, results on HawkI-Syn in Figure 5 show that StableZero123 is largely ineffective. HawkI fails to capture the correct camera elevation in all cases except for the house image. While Zero123++ handles both elevation and azimuth, it struggles with background and detailed features. For instance, the pyramid in the first row lacks shadow information; the waterfall image in the second row appears unnatural; and the house in the last row blurs detailed features. Conversely, our model accurately reflects shadow characteristics in the pyramid, and reconstructs the details and background of the waterfall and house examples from various viewpoints.

Similar observations are made for HawkI-Real results shown in Figure 6. StableZero123 is ineffective. Zero123++ fails to capture background or detailed information. For example, when tasked with camera control for an image of the Eiffel Tower, Zero123++ focuses solely on the Eiffel Tower, ignoring surrounding details. The original HawkI model, while producing aerial views, fails in angle conversion tasks. In contrast, our model accurately performs angle conversion tasks at $(30^\circ, 30^\circ)$ and $(30^\circ, 270^\circ)$, including the Seine River in the background for the Eiffel Tower image, showcasing its superiority. Camera control tasks for the HawkI-Real dataset, including images like the Hawaii beach and a cat, further demonstrate our model’s excellence compared to other models. The key benefits of our model over 3D-based NVS methods such as Zero123++ and 3D-free methods such as HawkI arises by merging the strengths of 3D-based techniques into a 3D-free optimization process, effectively combining the best features of both.

5.2 QUANTITATIVE EVALUATION

Following prior work Shi et al. (2023a); Kothandaraman et al. (2023); Liu et al. (2023a), we evaluate our method using six metrics - (i) LPIPS Zhang et al. (2018): Quantifies the perceptual similarity



Figure 8: **More Results on HawkI-Real.** We extend our analysis to additional settings of $(-20^\circ, 210^\circ)$ and $(-20^\circ, 330^\circ)$. Our model, when tested on the HawkI-Real dataset, demonstrated superior performance in view synthesis images, excelling in background inclusion and view consistency, and accurately representing the target elevation and azimuth angles. In comparison to other leading models such as Zero123++, HawkI, and StableZero123, our model’s results are notably better. StableZero123’s outputs are incomplete, and Zero123++ struggles with capturing background details and intricate information. Specifically, Zero123++ neglected surrounding details, focusing solely on the Eiffel Tower. The original HawkI model also failed to achieve the correct camera elevation or produced images that overlooked important features. For example, in the cat transformation task, the output incorrectly depicted three cats instead of two. Our model stands out by delivering exceptional results for the Eiffel Tower, Hawaiian beach, and cat transformations, underscoring its advanced capabilities over other models. Furthermore, we present a quantitative evaluation in Table 2, which confirms our model’s dominance over state-of-the-art benchmarks across various metrics.

between the generated and input images, with lower values indicating better performance. (ii) CLIP-Score Radford et al. (2021) and View-CLIP Score: Measure text-based alignment of the generated images. The CLIP score assesses alignment with both content and the $(\alpha_{\text{elev}}, \alpha_{\text{azi}})$ viewpoint, while the View-CLIP Score focuses specifically on the viewpoint. Higher values are preferred. (iii) CLIP-I Ruiz et al. (2023), CLIPD, and View-CLIPD: Evaluate image fidelity and directional similarity. CLIP-I measures the cosine similarity between the embeddings of multi-view images and the input image within the CLIP space. CLIPD¹ and View-CLIPD assess the consistency of transformations between two images, using text prompts similar to CLIP-Score and View-CLIP scores. Higher values are preferred. Similar to the quantitative comparison performed by Zero123++, we use 10% of the overall data from the HawkI-Syn and HawkI-Real datasets as the validation set to compute the quantitative metrics. Table 1 and Table 2 shows that our model significantly outperforms the state-of-the-art across these evaluation metrics, reinforcing how our models stands out by incorporating the robust features of 3D-based NVS methods into a 3D-free optimization strategy, thereby capitalizing on the benefits of both approaches.

6 CONCLUSIONS, LIMITATIONS AND FUTURE WORK

In this paper, we propose an approach that integrates the advantages of off-the-shelf 3D-based pre-trained models within 3D-free paradigms for novel view synthesis, offering precise control over camera angle and elevation. Our method performs effectively on complex, in-the-wild images containing multiple objects and background information. We qualitatively and quantitatively demonstrate the benefits of our method over corresponding 3D and 3D-free baselines. One limitation of our method is its reliance on an inference-time optimization routine for each scene and viewpoint, which may hinder real-time performance. Achieving faster performance is a direction for future work. Additionally, extending our approach to NVS and 3D applications with real-world constraints (such as respecting contact points and relative sizes) for tasks like editing, object insertion, and composition presents promising directions for further research. Based on the current results, we also propose

¹<https://huggingface.co/docs/diffusers/conceptual/evaluation>

Dataset, Angle, Method	LPIPS ↓	CLIP ↑	View-CLIP ↑	CLIPD ↑	View-CLIPD ↑	CLIP-I ↑
HawkI-Syn (30°, 30°) Ours	0.5667	29.9125	19.7100	0.0534	0.0568	0.8334
HawkI-Syn (30°, 30°) HawkI	0.5998	27.6516	18.6122	0.0405	0.0549	0.8108
HawkI-Syn (30°, 30°) Zero123++	0.5793	29.8709	18.4740	0.0552	0.0540	0.8330
HawkI-Syn (30°, 30°) Stable Zero123	0.6853	20.5335	18.0746	0.0528	0.0520	0.6181
HawkI-Syn (30°, 270°) Ours	0.5791	29.2654	19.1836	0.0553	0.0611	0.8274
HawkI-Syn (30°, 270°) HawkI	0.5996	29.0022	19.1088	0.0321	0.0498	0.8438
HawkI-Syn (30°, 270°) Zero123++	0.5911	28.9917	19.1491	0.0482	0.0597	0.7917
HawkI-Syn (30°, 270°) Stable Zero123	0.6441	21.2231	18.3738	0.0406	0.0403	0.6152
HawkI-Real (30°, 30°) Ours	0.6075	30.9333	20.7728	0.0829	0.0730	0.8333
HawkI-Real (30°, 30°) HawkI	0.6405	28.5431	18.5430	0.0506	0.0468	0.8302
HawkI-Real (30°, 30°) Zero123++	0.6679	29.8661	19.9530	0.0624	0.0467	0.8049
HawkI-Real (30°, 30°) Stable Zero123	0.6624	22.8604	18.7536	0.0523	0.0658	0.6740
HawkI-Real (30°, 270°) Ours	0.6180	30.0677	19.6756	0.0652	0.0709	0.8350
HawkI-Real (30°, 270°) HawkI	0.6497	28.4452	18.4231	0.0574	0.0577	0.8236
HawkI-Real (30°, 270°) Zero123++	0.6935	27.2773	19.5926	0.0605	0.0698	0.7212
HawkI-Real (30°, 270°) Stable Zero123	0.6466	23.6915	17.8817	0.0593	0.0658	0.6726

Table 1: **Quantitative Results.** Evaluation on six metrics demonstrate the superior results of our method over prior work.

Dataset, Angle, Method	LPIPS ↓	CLIP ↑	View-CLIP ↑	CLIPD ↑	View-CLIPD ↑	CLIP-I ↑
HawkI-Syn (-20°, 210°) Ours	0.5521	28.5599	17.9664	0.0502	0.0565	0.8535
HawkI-Syn (-20°, 210°) HawkI	0.5747	27.0915	16.9330	0.0403	0.0477	0.8370
HawkI-Syn (-20°, 210°) Zero123++	0.7193	23.9836	16.7291	0.0496	0.0886	0.7389
HawkI-Syn (-20°, 210°) Stable Zero123	0.6938	20.3084	16.8253	0.0403	0.0400	0.5826
HawkI-Syn (-20°, 330°) Ours	0.5672	29.1569	18.1494	0.0556	0.0535	0.8656
HawkI-Syn (-20°, 330°) HawkI	0.5967	27.6743	17.3102	0.0520	0.0529	0.8409
HawkI-Syn (-20°, 330°) Zero123++	0.6662	24.6859	17.5781	0.0688	0.0962	0.7383
HawkI-Syn (-20°, 330°) Stable Zero123	0.6201	22.3172	16.2088	0.0499	0.0542	0.7034
HawkI-Real (-20°, 210°) Ours	0.6222	29.6425	18.8914	0.0744	0.0709	0.7868
HawkI-Real (-20°, 210°) HawkI	0.6364	27.3844	17.5037	0.0568	0.0507	0.7821
HawkI-Real (-20°, 210°) Zero123++	0.7739	24.3284	18.7046	0.0713	0.0951	0.6798
HawkI-Real (-20°, 210°) Stable Zero123	0.6637	21.2952	17.2609	0.0556	0.0704	0.5829
HawkI-Real (-20°, 330°) Ours	0.6135	30.6951	18.9849	0.0506	0.0371	0.8500
HawkI-Real (-20°, 330°) HawkI	0.6500	28.5102	17.4244	0.0481	0.0315	0.8463
HawkI-Real (-20°, 330°) Zero123++	0.7132	25.5205	17.4653	0.0833	0.0977	0.7520
HawkI-Real (-20°, 330°) Stable Zero123	0.5730	23.9690	17.0343	0.0328	0.0726	0.7258

Table 2: **Quantitative Results.** Evaluation on six metrics demonstrate the superior results of our method over prior work.

exploring the use of an image-conditioned model to achieve a higher level of view consistency as a future research direction.

REFERENCES

- Anpei Chen, Zexiang Xu, Fuqiang Zhao, Xiaoshuai Zhang, Fanbo Xiang, Jingyi Yu, and Hao Su. Mvsnerf: Fast generalizable radiance field reconstruction from multi-view stereo. In *Proceedings of the IEEE/CVF international conference on computer vision*, pp. 14124–14133, 2021.
- Yiwen Chen, Chi Zhang, Xiaofeng Yang, Zhongang Cai, Gang Yu, Lei Yang, and Guosheng Lin. It3d: Improved text-to-3d generation with explicit view synthesis. In *Proceedings of the AAAI Conference on Artificial Intelligence*, volume 38, pp. 1237–1244, 2024.
- Ruiqi Gao, Aleksander Holynski, Philipp Henzler, Arthur Brussee, Ricardo Martin-Brualla, Pratul Srinivasan, Jonathan T Barron, and Ben Poole. Cat3d: Create anything in 3d with multi-view diffusion models. *arXiv preprint arXiv:2405.10314*, 2024.
- Lukas Höllein, Aljaž Božič, Norman Müller, David Novotny, Hung-Yu Tseng, Christian Richardt, Michael Zollhöfer, and Matthias Nießner. Viewdiff: 3d-consistent image generation with text-

-
- to-image models. In *Proceedings of the IEEE/CVF Conference on Computer Vision and Pattern Recognition*, pp. 5043–5052, 2024.
- Divya Kothandaraman, Tianyi Zhou, Ming Lin, and Dinesh Manocha. Aerialbooth: Mutual information guidance for text controlled aerial view synthesis from a single image. *arXiv preprint arXiv:2311.15478*, 2023.
- Junnan Li, Dongxu Li, Silvio Savarese, and Steven Hoi. Blip-2: Bootstrapping language-image pre-training with frozen image encoders and large language models. In *International conference on machine learning*, pp. 19730–19742. PMLR, 2023.
- Zhan Li, Zhang Chen, Zhong Li, and Yi Xu. Spacetime gaussian feature splatting for real-time dynamic view synthesis. In *Proceedings of the IEEE/CVF Conference on Computer Vision and Pattern Recognition*, pp. 8508–8520, 2024.
- Chen-Hsuan Lin, Jun Gao, Luming Tang, Towaki Takikawa, Xiaohui Zeng, Xun Huang, Karsten Kreis, Sanja Fidler, Ming-Yu Liu, and Tsung-Yi Lin. Magic3d: High-resolution text-to-3d content creation. In *Proceedings of the IEEE/CVF Conference on Computer Vision and Pattern Recognition*, pp. 300–309, 2023.
- Ruoshi Liu, Rundi Wu, Basile Van Hoorick, Pavel Tokmakov, Sergey Zakharov, and Carl Vondrick. Zero-1-to-3: Zero-shot one image to 3d object. In *Proceedings of the IEEE/CVF international conference on computer vision*, pp. 9298–9309, 2023a.
- Yuan Liu, Cheng Lin, Zijiao Zeng, Xiaoxiao Long, Lingjie Liu, Taku Komura, and Wenping Wang. Syncdreamer: Generating multiview-consistent images from a single-view image. *arXiv preprint arXiv:2309.03453*, 2023b.
- Ben Mildenhall, Pratul P Srinivasan, Matthew Tancik, Jonathan T Barron, Ravi Ramamoorthi, and Ren Ng. Nerf: Representing scenes as neural radiance fields for view synthesis. *Communications of the ACM*, 65(1):99–106, 2021.
- Dustin Podell, Zion English, Kyle Lacey, Andreas Blattmann, Tim Dockhorn, Jonas Müller, Joe Penna, and Robin Rombach. Sdxl: Improving latent diffusion models for high-resolution image synthesis. *arXiv preprint arXiv:2307.01952*, 2023.
- Ben Poole, Ajay Jain, Jonathan T Barron, and Ben Mildenhall. Dreamfusion: Text-to-3d using 2d diffusion. *arXiv preprint arXiv:2209.14988*, 2022.
- Guocheng Qian, Jinjie Mai, Abdullah Hamdi, Jian Ren, Aliaksandr Siarohin, Bing Li, Hsin-Ying Lee, Ivan Skorokhodov, Peter Wonka, Sergey Tulyakov, et al. Magic123: One image to high-quality 3d object generation using both 2d and 3d diffusion priors. *arXiv preprint arXiv:2306.17843*, 2023.
- Alec Radford, Jong Wook Kim, Chris Hallacy, Aditya Ramesh, Gabriel Goh, Sandhini Agarwal, Girish Sastry, Amanda Askell, Pamela Mishkin, Jack Clark, et al. Learning transferable visual models from natural language supervision. In *International conference on machine learning*, pp. 8748–8763. PMLR, 2021.
- Amit Raj, Srinivas Kaza, Ben Poole, Michael Niemeyer, Nataniel Ruiz, Ben Mildenhall, Shiran Zada, Kfir Aberman, Michael Rubinstein, Jonathan Barron, et al. Dreambooth3d: Subject-driven text-to-3d generation. In *Proceedings of the IEEE/CVF international conference on computer vision*, pp. 2349–2359, 2023.
- Robin Rombach, Andreas Blattmann, Dominik Lorenz, Patrick Esser, and Björn Ommer. High-resolution image synthesis with latent diffusion models. In *Proceedings of the IEEE/CVF conference on computer vision and pattern recognition*, pp. 10684–10695, 2022.
- Nataniel Ruiz, Yuanzhen Li, Varun Jampani, Yael Pritch, Michael Rubinstein, and Kfir Aberman. Dreambooth: Fine tuning text-to-image diffusion models for subject-driven generation. In *Proceedings of the IEEE/CVF conference on computer vision and pattern recognition*, pp. 22500–22510, 2023.

-
- Ruoxi Shi, Hansheng Chen, Zhuoyang Zhang, Minghua Liu, Chao Xu, Xinyue Wei, Linghao Chen, Chong Zeng, and Hao Su. Zero123++: a single image to consistent multi-view diffusion base model. *arXiv preprint arXiv:2310.15110*, 2023a.
- Yichun Shi, Peng Wang, Jianglong Ye, Mai Long, Kejie Li, and Xiao Yang. Mvdream: Multi-view diffusion for 3d generation. *arXiv preprint arXiv:2308.16512*, 2023b.
- Yujiao Shi, Hongdong Li, and Xin Yu. Self-supervised visibility learning for novel view synthesis. In *Proceedings of the IEEE/CVF Conference on Computer Vision and Pattern Recognition*, pp. 9675–9684, 2021.
- Matthew Tanik, Vincent Casser, Xinchen Yan, Sabeek Pradhan, Ben Mildenhall, Pratul P Srinivasan, Jonathan T Barron, and Henrik Kretzschmar. Block-nerf: Scalable large scene neural view synthesis. In *Proceedings of the IEEE/CVF Conference on Computer Vision and Pattern Recognition*, pp. 8248–8258, 2022.
- Peng Wang and Yichun Shi. Imagedream: Image-prompt multi-view diffusion for 3d generation. *arXiv preprint arXiv:2312.02201*, 2023.
- Jiale Xu, Xintao Wang, Weihao Cheng, Yan-Pei Cao, Ying Shan, Xiaohu Qie, and Shenghua Gao. Dream3d: Zero-shot text-to-3d synthesis using 3d shape prior and text-to-image diffusion models. In *Proceedings of the IEEE/CVF Conference on Computer Vision and Pattern Recognition*, pp. 20908–20918, 2023.
- Jiayu Yang, Ziang Cheng, Yunfei Duan, Pan Ji, and Hongdong Li. Consistnet: Enforcing 3d consistency for multi-view images diffusion. In *Proceedings of the IEEE/CVF Conference on Computer Vision and Pattern Recognition*, pp. 7079–7088, 2024.
- Richard Zhang, Phillip Isola, Alexei A Efros, Eli Shechtman, and Oliver Wang. The unreasonable effectiveness of deep features as a perceptual metric. In *Proceedings of the IEEE conference on computer vision and pattern recognition*, pp. 586–595, 2018.
- Chuanxia Zheng and Andrea Vedaldi. Free3d: Consistent novel view synthesis without 3d representation. In *Proceedings of the IEEE/CVF Conference on Computer Vision and Pattern Recognition*, pp. 9720–9731, 2024.
- Zhizhuo Zhou and Shubham Tulsiani. Sparsefusion: Distilling view-conditioned diffusion for 3d reconstruction. In *Proceedings of the IEEE/CVF Conference on Computer Vision and Pattern Recognition*, pp. 12588–12597, 2023.
- Zehao Zhu, Zhiwen Fan, Yifan Jiang, and Zhangyang Wang. Fsgs: Real-time few-shot view synthesis using gaussian splatting. *arXiv preprint arXiv:2312.00451*, 2023.

A APPENDIX



Figure 9: Additional comparisons in $(30^\circ, 30^\circ)$ and $(30^\circ, 270^\circ)$ settings on images from the Hawkl-Syn and Hawkl-Real datasets. Comparisons between the state-of-the-art view synthesis models, Zero123++, Hawkl, Stable Zero123, and our method highlights the superior performance of our model in terms of background inclusion, view consistency, and the accurate representation of target elevation and azimuth angles.

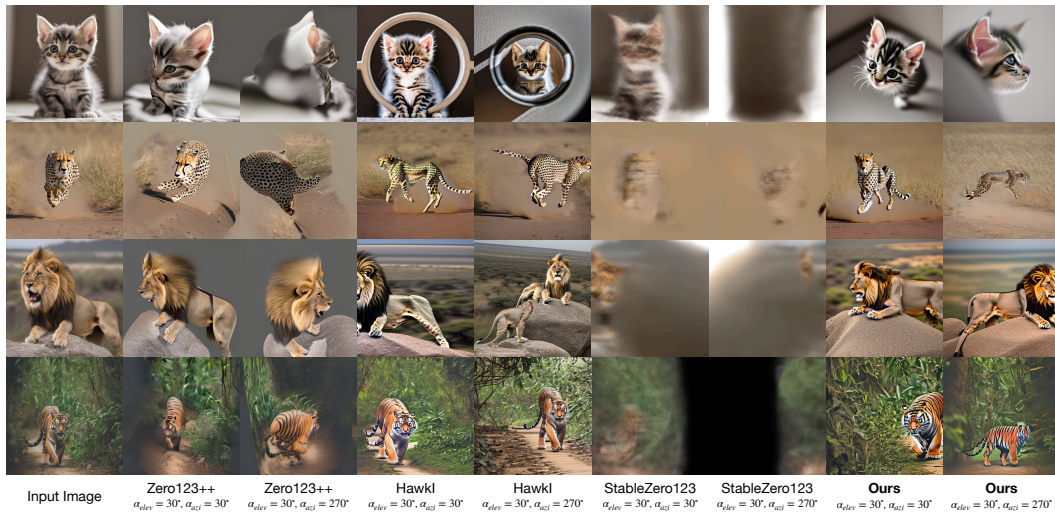


Figure 10: Additional comparisons in $(30^\circ, 30^\circ)$ and $(30^\circ, 270^\circ)$ settings on images from the Hawkl-Syn and Hawkl-Real datasets. Comparisons between the state-of-the-art view synthesis models, Zero123++, Hawkl, Stable Zero123, and our method highlights the superior performance of our model in terms of background inclusion, view consistency, and the accurate representation of target elevation and azimuth angles.



Figure 11: Additional comparisons in $(30^\circ, 30^\circ)$ and $(30^\circ, 270^\circ)$ settings on images from the HawkI-Syn and HawkI-Real datasets. Comparisons between the state-of-the-art view synthesis models, Zero123++, HawkI, Stable Zero123, and our method highlights the superior performance of our model in terms of background inclusion, view consistency, and the accurate representation of target elevation and azimuth angles.



Figure 12: Additional comparisons in $(30^\circ, 30^\circ)$ and $(30^\circ, 270^\circ)$ settings on images from the HawkI-Syn and HawkI-Real datasets. Comparisons between the state-of-the-art view synthesis models, Zero123++, HawkI, Stable Zero123, and our method highlights the superior performance of our model in terms of background inclusion, view consistency, and the accurate representation of target elevation and azimuth angles.